Key Points:
- CO_2-induced warming at the onset of PETM leads to reduced ventilation of the ocean interior, more pronounced in the Atlantic than in the Pacific Ocean
- Reduced ventilation results in accumulation of respiratory CO_2 and nutrients in intermediate waters, thereby lowering O_2
- Carbonate dissolution is triggered in ocean interior, while the surface remains supersaturated; asymmetry in the carbonate dissolution proxy record between the Pacific and Atlantic Oceans is thereby reproduced

Carbonate Dissolution Enhanced by Ocean Stagnation and Respiration at the Onset of the Paleocene-Eocene Thermal Maximum

Tatiana Ilyina[1] (ID) and **Mathias Heinze[1,2]**

[1] Max Planck Institute for Meteorology, Hamburg, Germany, [2] International Max Planck Research School on Earth System Modeling, Hamburg, Germany

Abstract The Paleocene-Eocene Thermal Maximum was a transient, carbon-induced global warming event, considered the closest analog to ongoing climate change. Impacts of a decrease in deepwater formation during the onset of the Paleocene-Eocene Thermal Maximum suggested by proxy data on the carbon cycle are not yet fully understood. Using an Earth System Model, we find that changes in overturning circulation are key to reproduce the deoxygenation and carbonate dissolution record. Weakening of the Southern Ocean deepwater formation and enhancement of ocean stratification driven by warming cause an asymmetry in carbonate dissolution between the Atlantic and Pacific basins suggested by proxy data. Reduced ventilation results in accumulation of remineralization products (CO_2 and nutrients) in intermediate waters, thereby lowering O_2 and increasing CO_2. As a result, carbonate dissolution is triggered throughout the water column, while the ocean surface remains supersaturated. Our findings contribute to understanding of the long-term response of the carbon cycle to climate change.

Plain Language Summary The Paleocene-Eocene Thermal Maximum, characterized by a relatively rapid carbon release to the atmosphere and global warming, has received ample scientific attention owing to its analogy to ongoing climate change. We perform Earth system model projections of concomitant changes in climate, ocean circulation, and marine biogeochemical cycles during the onset of the Paleocene-Eocene Thermal Maximum. In our simulations global warming (induced by atmospheric emissions of CO_2) leads to a weakening of the meridional overturning circulation and reduced ventilation of the ocean interior which is more pronounced in the Atlantic than in the Pacific Ocean. As a result of this ocean stagnation, respiratory CO_2 released via bacterial remineralization of organic matter (oxygen is thereby consumed) builds up in intermediate waters. This triggers carbonate dissolution and deoxygenation. This mechanism alone is sufficient to explain the asymmetry in the carbonate dissolution proxy record between the Pacific and Atlantic Oceans.

1. Introduction

The Paleocene-Eocene Thermal Maximum (PETM) is characterized in the geological record by a globally occurring concomitant negative excursion in carbon and oxygen isotope values of benthic foraminifera shells, vast dissolution of $CaCO_3$ sediments, and a mass extinction of marine benthic organisms. This evidence document the severity and abruptness of perturbation in the marine carbon cycle that is unprecedented over the last 100 million years (Thomas, 2007; Zachos et al., 2005), suggesting a very rapid carbon emission phase of less than 10 kyr (Turner et al., 2017; Zeebe et al., 2009). However, as some of the fundamental processes to explain the PETM sediment archives are not identified yet, there are still several unknowns related to this period in Earth's history.

For instance, the deep ocean during the PETM was affected by varying degrees of ocean acidification. The deep-sea carbonate dissolution pattern displays a much stronger dissolution in the Atlantic Ocean than in the Pacific Ocean (Thomas et al., 2002; Zachos et al., 2005; Zeebe & Zachos, 2007). While the Pacific carbonate compensation depth (CCD) shoaled only several hundred meters, the Atlantic Ocean experienced a CCD shoaling of ~2 km (Zeebe et al., 2009). A similar pattern is observed for oxygen distributions, promoting suboxic conditions in the Atlantic Ocean while the Pacific Ocean stayed oxygenated throughout the whole event (Palike et al., 2014). The mechanism behind the different responses of the two basins remains speculative.

The most reasonable explanation is represented so far by an Atlantic source of methane (Dickens et al., 1995), in some cases in conjunction with a circulation reversal (Zeebe et al., 2009), which would trigger strong $CaCO_3$ dissolution and oxygen consumption (through methane oxidation) in the Atlantic itself, while the Pacific would only partially be affected. A modeling study showed furthermore that a reduction in Atlantic sediment bioturbation would increase dissolution intensity in the Atlantic sites (Panchuk et al., 2008).

Another unknown related to the PETM geological record is the contrast in response of surface and deep ocean carbonate chemistry. Most planktic calcareous foraminifera and nannoplankton taxa showed rapid evolutionary turnover, but no major extinction during the PETM (Gibbs, Bown, et al., 2006; Thomas, 2007). In contrast, about 30–50% of species of benthic foraminifera went extinct, suggesting inhospitable conditions in the deep ocean (Thomas, 2007). Along with ocean acidification, benthic organisms have probably also been exposed to the effects of multiple stressors, such as warming, reduced food supply, and low-oxygen conditions.

Climate change-induced ocean circulation changes have been suggested for the PETM in both proxy and modeling studies (Lunt et al., 2010; Nunes & Norris, 2006; Tripati & Elderfield, 2005). Circulation changes in turn must have affected ocean biogeochemistry analogous to future projections (Bopp et al., 2013). Previous modeling studies investigated the response of the ocean carbon cycle to the PETM carbon perturbation (Panchuk et al., 2008; Ridgwell & Schmidt, 2010; Zeebe et al., 2009). Until now, however, the effects of transient changes in ocean circulation on the organic (Winguth et al., 2012) and inorganic (Alexander et al., 2015) carbon cycles have been addressed separately and thus interactions between them remain poorly quantified. Yet interactions between inorganic and organic components of the ocean carbon cycle have the potential for producing synergistic effects in the response of ocean biogeochemistry to climate change. For instance, microbial remineralization of organic nutrients consumes oxygen and releases CO_2, thereby increasing dissolved inorganic carbon (DIC) and decreasing carbonate saturation state. Could changes in large-scale ocean circulation and concurrent changes in the inorganic and organic carbon cycles explain the asymmetry in horizontal gradients in $[O_2]$ and $[CO_3^{2-}]$, as well as vertical gradients in carbonate chemistry during the PETM?

We address this question using a state-of-the-art Earth System Model (Giorgetta et al., 2013; Max-Planck-Institute for Meteorology Earth System Model [MPI-ESM]; see section 2) which enables us to study the effect of changes in the ocean circulation on the marine carbon cycle during the onset of the PETM.

2. Methods

Model Setup. We address the PETM carbon perturbation, using the MPI-ESM (Giorgetta et al., 2013) in a configuration similar to that used within the fifth phase of the Coupled Model Intercomparison Project (CMIP5) but with a coarser spatial resolution. The model is integrated with a time step of 2.4 hr with a spatial resolution of 3.5° and 31 and 40 vertical levels in the atmosphere and ocean compartments, respectively. The model uses a Paleocene-Eocene topography (Bice & Marotzke, 2001), which has been already used in several other PETM modeling studies (Panchuk et al., 2008; Zeebe et al., 2009). MPI-ESM consists of the atmospheric general circulation model ECHAM6, the land surface and vegetation model JSBACH, and the ocean general circulation model MPIOM. The ocean biogeochemistry part of the ESM is based on the HAMburg Ocean Carbon Cycle model, HAMOCC (Ilyina et al., 2013). The distributions of tracers are not restored to any kind of data set throughout the simulation, to be consistent with the biological, chemical, and physical dynamics of the model. HAMOCC is coupled online to MPIOM (for computing tracer advection and mixing) and simulates 18 biogeochemical tracers prognostically within a three-dimensional ocean circulation state. Moreover, MPIOM provides temperature, pressure, and salinity fields, which are used to calculate various transformation rates and chemical constants within HAMOCC.

Biological processes are based on an extended nutrient-phytoplankton-zooplankton-detritus-type model. The colimitation of phosphate, nitrate, and iron, together with temperature and radiation, determines primary production in HAMOCC. Since the biogeochemical processes are calculated on the basis of phosphorous, the Redfield ratio (P:N:C:O_2 ratio of 1:16:122:172) is used to calculate the associated changes in the remaining tracer concentrations. Biological products (opal, $CaCO_3$, and particulate organic carbon [POC]) are transported to depth via prescribed vertical sinking rates and are simultaneously subject to advective and diffusive processes. Particles undergo constant remineralization, distributing silicate, DIC, total alkalinity (TA), and nutrients (while decreasing oxygen) throughout the water column. Aerobic remineralization of POC takes place in waters with oxygen concentrations >0.5 μmol O_2/L. If oxygen falls below a certain concentration, decomposition of POC by denitrification (<0.5 μmol O_2/L) and sulfate reduction (<3 μmol O_2/L) sets in.

The formation of $CaCO_3$ shells consumes DIC and TA in a molar ratio of 1:2. The $CaCO_3$ formation rate linearly depends on the calcite saturation state (Ω) in the surface ocean (Ilyina et al., 2009). The dissolution of $CaCO_3$ at depth is a function of Ω and a dissolution rate constant (Ilyina & Zeebe, 2012). Ω is calculated from the apparent solubility product of calcite, which is based on temperature, pressure, $[CO_3^{2-}]$, and constant $[Ca^{2+}]$. The globally averaged DIC/TA ratio in the pre-PETM background state is 2.235/2.325 (0.961), which is close to the preindustrial ratio in MPI-ESM.

HAMOCC includes a sediment module, calculating the same tracer distributions as in the water column. It consists of 12 vertical layers, spreading over the uppermost 14 cm of the sediment. Major processes simulated in the sediment are vertical diffusion of porewater, decomposition of POC, as well as dissolution of opal and $CaCO_3$. Below the active sediment there is one diagenetically consolidated (burial) layer representing the bedrock. The burial output of $CaCO_3$, organic matter, and silicate is accounted for by globally homogeneous weathering input. Weathering input is chosen to balance the sediment output during the spin-up of the Late Paleocene background climate state and is kept constant during the PETM simulation.

Pre-PETM Background Climate. The late Paleocene background ocean biogeochemistry state was spun up from basin-wide mean concentrations in an ocean stand-alone simulation of 3,200 years (Heinze & Ilyina, 2015), followed by an additional 3000-year spin-up simulation in the fully coupled mode. In total, the model spin-up simulation was longer than 6,000 years, which is sufficient to ventilate the whole ocean at least once. Thereby, we follow a spin-up protocol that is commonly used in CMIP-type simulations and is compliant with the international standards applied to coupled model simulations (Séférian et al., 2016). Note that with this approach we address only the onset of the PETM, not the whole event.

CO_2 Increase Scenarios. We start our simulation from a late Paleocene background state with the atmospheric CO_2 concentration of 560 ppm (Heinze & Ilyina, 2015). To match an annual carbon emission of 1 Gt C (which is 1 order of magnitude lower than the estimated total anthropogenic CO_2 emissions for the year 2017; Le Quéré et al., 2018), we linearly increase the atmospheric CO_2 concentration by 0.47 ppm/year, resulting in a nearly doubling of atmospheric CO_2 concentrations after 1,300 years. From year 1,300 on, the atmospheric CO_2 is held constant at the value of 1170 ppm. Our model configuration is concentration driven, such that land and ocean carbon uptake do not feedback on the atmospheric CO_2 concentrations or the climate. However, uptake by these reservoirs equals 1,419 Gt C over the simulation period of 5,000 years. This results in a total "compatible emission" of 2,719 Gt C in the standard PETM run (see supporting information for detailed description).

Additionally to the standard PETM run, we carried out an idealized *no-warming* sensitivity simulation, analogous to the idealized CMIP5 scenarios used to infer carbon-climate feedbacks (Ilyina et al., 2013). Here we prescribe the same atmospheric CO_2 increase as in the standard PETM simulation, but CO_2 is treated as a non-radiatively active gas, meaning that its increase does not produce additional warming (CO_2 is fixed to 560 ppm in the radiation code of the model). This experiment follows the set of idealized CMIP5 simulations with the same type of models that we have used in our study (e.g., Arora et al., 2013). The purpose of such sensitivity analysis is to isolate the carbon cycle response to climate change from the response to CO_2 increase (IPCC, 2013). By analyzing the differences between the no-warming and the standard PETM run, we can isolate the effects of climate change on the marine carbon cycle. Note that Ω is directly related to temperature, which produces slightly higher $CaCO_3$ dissolution in the no-warming scenario relative to the standard PETM run. This idealized simulation ran for a period of 1,500 years, including 200 years of stable atmospheric CO_2 concentrations.

3. Results and Discussion

3.1. Climate Sensitivity

In our simulation, after doubling atmospheric CO_2 concentration (year 1187), the effective climate sensitivity is 5.3 °C (indicated by surface temperature change). After 1,300 model years atmospheric CO_2 concentration is increased by ~110%, in comparison to its initial value, which results in a surface warming of 5.75 °C. At the end of the simulation (year 5000) the surface warming amounts to 8.3 °C. The equilibrium climate sensitivity of the same model used within CMIP5 with a higher spatial resolution (MPI-ESM: 1.5° horizontal resolution, 47 vertical level) in a present-day setup is 3.1 °C (Mauritsen et al., 2012).

There is growing scientific evidence that climate sensitivity increases in warmer climates due to a strengthening of the water vapor feedback with increasing surface temperatures (Meraner et al., 2013; Popp et al., 2016).

During the early Paleogene, radiative forcing by CO_2 deviates significantly from pure logarithmic behavior, as it is assumed for modern conditions (Caballero & Huber, 2013; González et al., 2018). According to these studies, the climate sensitivity during the Paleocene-Eocene epoch was most probably higher than today's. Thus, the higher climate sensitivity in our PETM model in comparison to the modern climate model version (from CMIP5) is expectable given the growing body of scientific evidence on this topic. The climate sensitivity of the Eocene is very uncertain; this is also why in our study we do not attempt to constrain the absolute amount of carbon necessary to drive the PETM. On the contrary, there is higher confidence in global temperature increase at the onset of the PETM. Proxies for surface temperatures seem to be more reliable than reconstructions of atmospheric $[CO_2]$.

3.2. Changes in Hydrological Cycle and Ocean Circulation

The background state, from which the PETM perturbation scenario starts, is based on an atmospheric CO_2 concentration of 560 ppm, which produces a late Paleocene climate state (see Figure S2) in accordance with proxy data (Dunkley Jones et al., 2013). For the onset of the PETM, the atmospheric CO_2 is prescribed with an increase rate equivalent to an annual carbon pulse of 1 Gt C. Over a period of 1,300 years this leads to atmospheric CO_2 concentrations of about 1,170 ppm. Such annual carbon emission rates are consistent with recent proxy interpretations (Bowen et al., 2015; Hoenisch et al., 2012; Penman et al., 2014) that infer peak emission rates of ≥ 1 Gt C/year for the main phase of the PETM. As a result of rising CO_2 in our scenario, the globally averaged sea surface temperature (SST) increases by ~7 °C over the simulation period of 5,000 years (Figure 1c). Consistent with proxy record analysis, high-latitude SST increases by 8 to 10 °C (proxies: 4–9 °C; Kennett & Stott, 1991; Sluijs et al., 2006; Sluijs et al., 2011), while the tropical SST rises by about 6 °C (proxies: ~5 °C; Zachos et al., 2003).

The net freshwater flux into the ocean increases due to the prescribed CO_2 rise and concomitant warming. In general, the tropics and middle to high latitudes experience a greater freshwater input, while in the subtropics the net loss of freshwater due to evaporation is increased (Figure S3). Available reconstructions imply that substantial shifts in the hydrological cycle occurred during the PETM (McInerney & Wing, 2011), albeit the resulting changes have been regionally very inconsistent (Chen et al., 2016).

Pre-PETM deepwater formation areas in the Pacific and Indian sectors of the Southern Ocean receive an increase in freshwater input by 48% and 43%, respectively (Figure S4). Due to increased precipitation and warming, high-latitude surface waters are less dense and hence increase their stability. As a result, convective processes decrease. Especially in the Southern Hemisphere high latitudes the mixed layer depth shoals strongly (Figure S3), which is in accordance to the increased freshwater input in the deepwater formation areas. An intensification of the hydrological cycle and especially an increase in high-latitude freshwater input due to PETM warming are the main reasons for ocean stratification (Huber et al., 2003).

In response to surface warming and freshwater input, the Meridional Overturning Circulation (MOC) weakens abruptly in the Southern Hemisphere (Figure 1c). The maximum strength in density driven MOC (below 1,000-m depth) decreases from on average 18 Sv to a minimum value of 6 Sv in year 1500 after the onset of the carbon perturbation. From this point on the MOC appears to recover slowly, due to some strengthening of deep convection in the Indian and Atlantic sectors of the Southern Ocean. Convection-induced sinking of water masses occurs in the Pacific and Indian sectors of the Southern Ocean. The Northern Hemisphere lacks a North Atlantic Deepwater cell and North Pacific deepwater formation (Figure 1a). Such a Southern Hemisphere-driven ocean circulation is supported by several proxy record studies (Hague et al., 2012; Nunes & Norris, 2006; Thomas et al., 2003; Tripati & Elderfield, 2005).

Interpretations by Tripati and Elderfield (2005) suggest a decrease in Southern Ocean deepwater formation during the onset of the PETM. However, Tripati and Elderfield also interpret $\delta^{13}C$ from Central Pacific sites (ODP 865 and ODP 1209) to indicate relatively young water in comparison to DSDP site 527 in the Atlantic sector of the Southern Ocean. They associate these findings to a gradual development of a circulation cell in the North Pacific throughout the PETM. In our simulation North Pacific deepwater production does not evolve. Instead, some deepwater formation persists in the Indian Ocean sector of the Southern Ocean. This water is transported in middepth along the northern Australian continent into the Central Pacific, which represents another option to produce the temperature and carbon isotope signal at the Pacific sites. Additionally, Nunes and Norris (2006) interpret from $\delta^{13}C$ a weakening in Southern Ocean deepwater formation, accompanied by a possible switch in main convection areas. Their results suggest that the most significant contribution of deep water came from the Northern Hemisphere or Pacific during the PETM. However, they are missing
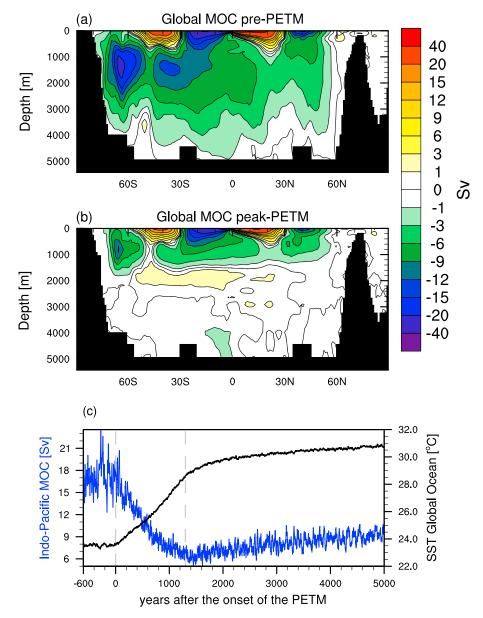
Figure 1. Response of the meridional overturning circulation and sea surface temperature to PETM warming. (a) Stream function of the globally averaged MOC (Sv) for the pre-PETM setting. Positive values correspond to clockwise circulation. (b) Globally averaged MOC at the end of the PETM simulation (mean over last 30 simulation years). (c) Time series of the South Pacific MOC (absolute values, 10-year running mean, blue line) and the global SST (black line) over the whole experiment. Negative years refer to the pre-PETM background state. Dashed gray lines indicate the beginning and termination of atmospheric CO_2 increase, respectively. PETM = Paleocene-Eocene Thermal Maximum; MOC = Meridional Overturning Circulation; SST = sea surface temperature.

a high-latitude sample site in the Pacific Ocean. The Pacific basin in their study is only represented by an equatorial site. Also, previous modeling studies support an ocean circulation dominated by Southern Ocean deep and bottom water formation under late Paleocene conditions (Alexander et al., 2015; Bice & Marotzke, 2002; Lunt et al., 2012; Panchuk et al., 2008; Winguth et al., 2012). An increase in CO_2 then leads to enhanced stratification and a weakening of deep and bottom water formation as shown in our results.

As soon as both the CO_2 and the freshwater forcing become stationary in our simulation, the MOC equilibrates at 9 Sv from year 4000 on. Beyond the atmospheric CO_2 increase phase, nearly no deepwater formation takes place below 2000-m depth (Figure 1b). The rather weak MOC and shallow convection that result from our simulation are consistent with other modeling studies (Lunt et al., 2010) and interpretations of the $\delta^{13}C$ and
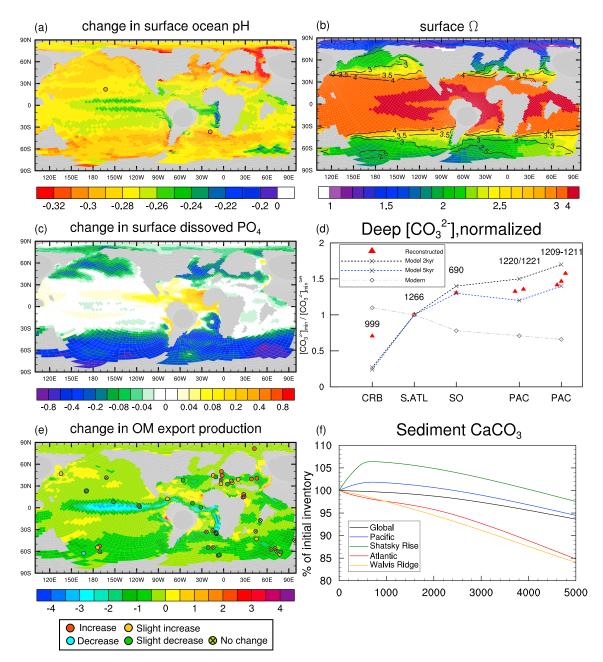
Figure 2. Changes in ocean biogeochemistry at the sea surface, in the deep ocean and sediments. (a) Anomaly (calculated as difference between peak PETM and pre-PETM state) in surface pH, overlain with pH reconstructions (Penman et al., 2014). (b) Surface distribution of calcite saturation state (Ω, mean over the last 30 simulation years). Contour lines show surface Ω of the pre-PETM background state. (c) Anomaly in surface dissolved phosphate (PO_4, µmol/L). (d) Simulated deep-sea CO_3^{2-} basin gradient at 2 and 5 kyr after the onset of the PETM and reconstructions (Zeebe & Zachos, 2007), both based on site-specific minimum $[CO_3^{2-}]$ normalized to S.ATL site. CRB = Caribbean; S.ATL = South Atlantic Ocean; SO = Southern Ocean, PAC = Pacific Ocean. (e) Anomaly in export production (mol C·m^{-2}·year^{-1}), overlain with productivity tendencies from reconstructions (Winguth et al., 2012). (f) Change in $CaCO_3$ sediment content over the whole sediment depth of the model (percent of pre-PETM inventory) for specific regions. Shatsky Rise and Walvis Ridge region are defined in supporting information Figure S5. Note the nonlinear color scales in subplots (c) and (b). PETM = Paleocene-Eocene Thermal Maximum; OM = organic matter.

paleotemperature proxy record (Tripati & Elderfield, 2005) indicating greater stratification during the PETM in the Southern Ocean.

3.3. Impacts on Marine Biology and Carbonate Chemistry

Enhanced thermal stratification affects the biology and carbonate chemistry of the surface ocean. The oceans generally reveal a weaker nutrient supply to the surface (Figure 2c), except in the regions that are controlled by the eastern boundary currents in the subtropical Pacific and Atlantic. The reduced nutrient availability affects
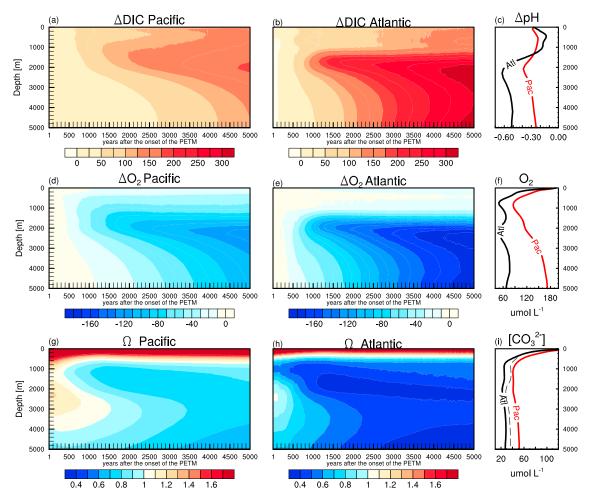
Figure 3. Ocean biogeochemistry response to biological respiration processes in a poorly ventilated ocean of the PETM. Temporal evolution of DIC anomaly averaged over (a) the Pacific and (b) the Atlantic basin. (c) Depth profile of pH anomaly (peak PETM and pre-PETM) averaged over the Pacific (red line) and the Atlantic Oceans (black line). Temporal evolution of oxygen (O_2) anomaly averaged over (d) the Pacific and (e) the Atlantic basins. (f) Depth profiles of oxygen concentration (mean over last 30 simulation years). Temporal evolution of Ω averaged over (g) the Pacific and (h) the Atlantic basins. (i) Depth profile of $[CO_3^{2-}]$; dashed line indicates South Atlantic $[CO_3^{2-}]$. All concentrations are given in micromole per liter. PETM = Paleocene-Eocene Thermal Maximum; DIC = dissolved inorganic carbon.

export production, which decreases globally by ∼30% in our simulation. The model captures the productivity decrease due to weakened upwelling in the equatorial Pacific (Figure 2e) and matches the reconstructions for large parts of the Atlantic and Indian Oceans, showing little to no change in export production. Several observational sites in the Tethys Ocean infer an increase in export production, while our simulation shows strong increase only along the eastern boundary of the basin. Increased weathering rates due to an intensification in extratropical precipitation during the PETM could have potentially washed out more nutrients (Winguth et al., 2012), triggering additional production. However, the production increase did not compulsively set in at the onset of the event but could have contributed to CO_2 drawdown during the termination of the PETM (Bains et al., 2000). Another factor that could have affected productivity of the PETM ocean is ocean acidification. In our simulation ocean acidification decreases production of $CaCO_3$ (according to Ilyina et al., 2009), thereby further contributing to the overall decrease in productivity.

The surface ocean Ω decreases with increasing atmospheric CO_2 (Figure 2b) but stays >1 throughout the whole simulation. Our results are consistent with proxy studies suggesting oligotrophic and supersaturated with respect to $CaCO_3$ surface waters conditions (Gibbs, Bralower, et al., 2006) that ensured survival of the most calcareous nannoplankton taxa during the PETM (Gibbs, Bown, et al., 2006). The globally averaged decrease in surface pH by 0.28 matches recent boron isotope-derived pH reconstructions (Penman et al., 2014; Figure 2a).

Carbonate chemistry of the high-latitude regions is affected most strongly by CO_2 increase due to relatively cold waters and naturally lower carbonate buffering capacity.

The poorly ventilated PETM ocean results in weakened vertical transport of carbon by oceanic mixing. However, our model results show that DIC increases in response to rising atmospheric CO_2. Surprisingly, the largest increase is found at intermediate depths, between 1,000- and 2,000-m depths (Figures 3a and 3b). Likewise, oxygen concentration decreases throughout the water column over time (Figures 3d and 3e), showing a similar pattern to the DIC concentration increase. This suggests remineralization processes to be the main trigger of deoxygenation and carbon accumulation. Reduced mixing weakens the resupply of nutrients and DIC, which are released during remineralization, to the surface. Instead, low-oxygen and high-DIC waters resulting from decomposition of biologically produced organic matter are trapped in the ocean interior. This promotes strong deoyxgenation and ocean acidification (Figure 3). The accumulation of metabolic CO_2 leads to corrosive conditions with respect to $CaCO_3$ throughout the water column (Figure 3g,h) and triggers sedimentary $CaCO_3$ dissolution. Although export production decreases by 30%, there is still sufficient supply of OM to drive this metabolic CO_2 buildup in the ocean interior. Ultimately, it is the atmospheric CO_2 that drives the PETM-related perturbation in the carbon cycle. However, the weakening in MOC and the associated reduction in the physical carbon pump (Zachos et al., 2008) are compensated by a biologically induced process (i.e., microbial respiration) to drive $CaCO_3$ undersaturation at depth, despite a thermally induced more stable stratification.

3.4. Response of Sedimentary $CaCO_3$

The Paleocene-Eocene background sediment in our simulation consists of a solid $CaCO_3$ inventory of 1,963 Gt C, which is slightly higher than estimates from present-day modeling (1,610 Gt C, CMIP5 simulation with MPI-ESM) and observations (1,600 Gt C; Archer, 1996). The model captures the spatial pattern of the compiled sediment core data reasonably well (Figure S5a). While the North Atlantic and the central Pacific Ocean match the observations quite well, the $CaCO_3$ abundance in the Walvis Ridge area is somewhat underestimated by the model. The mismatch in $CaCO_3$ deposition in the eastern Pacific and the central Indian Ocean can mainly be explained by divergences in depth between the cores and the model bathymetry. For instance, the 0 wt% sediment cores in the Indian Ocean display the $CaCO_3$ content between 4,000 and 4,900 m in depth. The applied bathymetry is several 100 m shallower in these locations (Heinze & Ilyina, 2015). While data and model results look consistent in the Pacific sector of the Southern Ocean, the model generally seems to underestimate the late Paleocene $CaCO_3$ abundances in the Atlantic and Indian sectors of the Southern Ocean.

Sediment distributions at the end of the 5000 year PETM simulation show an overall decrease in $CaCO_3$ wt%. Weak dissolution of $CaCO_3$ in the Southern Ocean is principally in line with the data record, as well as the simulated dissolution response in the North Atlantic Ocean. The sediment record indicates strong dissolution of $CaCO_3$ in the eastern Pacific (ODP sites 1220/1221). Yet there is no dissolution occurring in our simulation, since the eastern Pacific did not show any larger $CaCO_3$ deposits in our late Paleocene state. If we look at the entire ocean basin inventories, the Pacific and Atlantic $CaCO_3$ dissolution pattern resulting from our simulation conforms with moderate CCD shoaling in the Pacific and strong CCD shoaling in the Atlantic (Zachos et al., 2005; Zeebe et al., 2009). While the Pacific decrease in $CaCO_3$ sediments amounts to only 5.8%, it decreases about 15% in the Atlantic Ocean within the 5,000 years of the PETM experiment. However, the pointwise comparison of our results to sediment core data shows that the Shatsky Rise dissolution could be more moderate in our simulation. In the Atlantic Ocean $CaCO_3$ sediments decline, but Walvis Ridge sediments still contain $CaCO_3$, albeit dissolution enhances throughout the simulation (Figure 2f). The dissolution of sedimentary $CaCO_3$ depends on the chemical composition of the overlying seawater at the ocean-sediment boundary layer. It takes tens of thousands of years for the sediments to record the water column carbonates evolution correspondingly (Heinze et al., 1999). So within our 5,000 years of simulation, the model does not yet reproduce the full history of the Shatsky Rise and Walvis Ridge sediment cores. We note also that the sedimentary records from Walvis Ridge are likely less representative for the onset of the PETM due to the so-called dissolution burndown effect that could have erased the onset signal (Kelly et al., 2010).

Apart from the time issue (our sediment state is the result of 5,000 simulation years vs. 150,000 years in the sediment record), the sediment $CaCO_3$ state depends on diverse factors, such as bathymetry and the background $CaCO_3$ sediment state, which introduces large uncertainties into the pointwise model-data comparison. Furthermore, another huge uncertainty hampering the pointwise model-data comparison comes

with the reconstructions of the exact paleocoordinates of the sediment cores. Divergent paleogeographic reconstructions of sample sites introduce large uncertainty into model-data comparison (Huber & Caballero, 2011). In order to illustrate that the model does have the right tendencies toward reproducing the Shatsky Rise and Walvis Ridge sediment records, we integrated the $CaCO_3$ sediment inventory over the area given by the spread in sediment core position reconstructions for Shatsky Rise (Pacific Ocean, ODP sites 1209–1212; Colosimo et al., 2006) and Walvis Ridge (Atlantic Ocean, ODP sites 1262–1267; Zachos et al., 2005). The inventory change over these areas clearly shows a much stronger $CaCO_3$ decrease in the Walvis Ridge area than in the Shatsky Rise area in our results (Figure 2f; for integration area see black rectangles in Figure S5).

3.5. Asymmetry in Basin Patters of Carbonate Dissolution

Changes in ocean circulation can explain yet another conundrum of the PETM, namely, the asymmetry in $CaCO_3$ sediment dissolution between the Atlantic and Pacific basins. Using Shatsky Rise and Walvis Ridge core data, Zeebe and Zachos (2007) inferred that $[CO_3^{2-}]$ must have been 1.5 times higher in the Pacific than in the South Atlantic during the main dissolution phase of the PETM indicating a reverse $[CO_3^{2-}]$ gradient relative to the modern ocean.

Our model results clearly show a strong gradient in $CaCO_3$ undersaturation between the Pacific and the Atlantic seawater at depth. Especially in the sluggish Atlantic, the OM remineralization rather than the physical mixing from the surface keeps the deep ocean rich in carbon. In the Pacific, some deep-sea ventilation persists throughout the PETM simulation, causing only weak accumulation of metabolic CO_2. Consequently, the overall $CaCO_3$ dissolution is higher in the Atlantic than in the Pacific (Figure 2f). As a result, the horizontal $[CO_3^{2-}]$ basin gradient of 1.5:1 between the South Atlantic and Pacific suggested by Zeebe and Zachos (2007) and Zeebe et al. (2009) is reproduced in our simulation (Figures 2d and 3i), without prescribing additional deep ocean ventilation or ocean carbon sources (Thomas et al., 2002; Zeebe et al., 2009). Additionally, the more intense accumulation of low-oxygen waters resulting from OM remineralization can explain why deoxygenation was stronger in the Atlantic than in the Pacific during the PETM (Figure 3f), suggested by recent proxy studies (Palike et al., 2014).

3.6. Idealized No-Warming Model Scenario

To confirm our findings on the role of circulation, we performed an idealized simulation with the same atmospheric CO_2 increase rate. However, in this simulation the additional CO_2 does not feedback on the radiation of the atmospheric component of the model (the no-warming scenario; see section 2). As a result, the deep sea remains ventilated throughout the simulation. Although the global $CaCO_3$ sediment dissolution increases by 19% in comparison to the standard PETM run in response to more efficient CO_2 invasion, undersaturation and sediment dissolution are much weaker in the Atlantic under unimpaired deep ocean ventilation (Figure S6). In comparison to our standard PETM simulation, the $[CO_3^{2-}]$ decrease is much weaker. Hence, stagnation of the ocean mixing and subsequent accumulation of metabolic CO_2 are essential to establish corrosive deep-sea conditions in the Atlantic. Moreover, in the Pacific and Indian Oceans the strength of the circulation and mixing in the no-warming scenario enhances the undersaturation of the deep ocean, triggering stronger sedimentary $CaCO_3$ dissolution. Consequently, CCD shoaling would be stronger in the Pacific than in the Atlantic without enhancement of ocean stratification.

The results of the conducted sensitivity study emphasize the role of the climate change effects on the marine carbon cycle in producing the different responses in deep-sea $[CO_3^{2-}]$ between Atlantic and Pacific Oceans. Moreover, this experiment confirms that it is due to the circulation changes that the enhancement of respiratory CO_2 takes place. These findings are supported by two additional sensitivity experiments, in which a higher CO_2 increase rate and an ocean CO_2 source is considered, respectively (see section S3). In a higher CO_2 scenario, a too strong SST increase and a too strong decrease in pH are produced (Figure S7) that are not in agreement with proxy record. In a scenario with an additional CO_2 source in the deep Atlantic (as suggested by, e.g., Dickens et al., 1995; Zeebe et al., 2009), the resulting deep-sea $CaCO_3$ is 7 times higher in the Pacific than in the South Atlantic (Figure S10) which is likewise not in agreement with the proxy record.

4. Summary and Conclusions

We present projections of concomitant changes in climate, ocean circulation, and marine biogeochemical cycles during the onset of the PETM with an ESM based on the ocean and atmospheric general circulation models. By applying the very same tools that we use in future climate change projections that serve to inform the IPCC process, we suggest a so far poorly assessed mechanism of carbon invasion into the deep ocean

of the PETM. This mechanism works as follows. Global warming (induced by atmospheric emissions of CO_2) leads to a weakening of the MOC and reduced ventilation of the ocean interior which is more pronounced in the Atlantic Ocean than in the Pacific Ocean. As a result of this ocean stagnation, respiratory CO_2 released via bacterial remineralization of organic matter (oxygen is thereby consumed) builds up in intermediate waters. This triggers carbonate dissolution and deoxygenation of the ocean interior while the surface ocean remains supersaturated with respect to $CaCO_3$. Moreover, the accumulation of metabolic CO_2 is more pronounced in the Atlantic Ocean, since the Pacific Ocean is better ventilated, causing the asymmetry in the $CaCO_3$ suggested by the sediment record. This mechanism alone (without prescribing additional carbon sources or deep ocean ventilation) is sufficient to explain the basin gradient in the carbonate dissolution proxy record between the Pacific and Atlantic Oceans. Hence, reorganization of ocean circulation and concomitant metabolic CO_2 accumulation should be considered when interpreting proxy data as a pathway of carbon invasion into the deep ocean during the PETM. Furthermore, this mechanism will likely become increasingly important in the future warming climate, on centennial to millennial timescales.

References

Alexander, K., Meissner, J. K., & Bralower, J. T. (2015). Sudden spreading of corrosive bottom water during the Palaeocene-Eocene thermal maximum. *Nature Geoscience*, *8*(6), 458–461. https://doi.org/10.1038/ngeo2430

Archer, D. E. (1996). An atlas of the distribution of calcium carbonate in sediments of the deep sea. *Global Biogeochemical Cycles*, *10*(1), 159–174. https://doi.org/10.1029/95GB03016

Arora, V. K., Boer, G. J., Friedlingstein, P., Eby, M., Jones, C. D., Christian, J. R., et al. (2013). Carbon-concentration and carbon-climate feedbacks in CMIP5 Earth system models. *Journal of Climate*, *26*(15), 5289–5314. https://doi.org/10.1175/JCLI-D-12-00494.1

Bains, S., Norris, R. D., Corfield, R. M., & Faul, K. L. (2000). Termination of global warmth at the Palaeocene/Eocene boundary through productivity feedback. *Nature*, *407*(6801), 171–174. https://doi.org/10.1038/35025035

Bice, K. L., & Marotzke, J. (2001). Numerical evidence against reversed thermohaline circulation in the warm Paleocene/Eocene ocean. *Journal of Geophysical Research*, *106*(C6), 11,529–11,542. https://doi.org/10.1029/2000JC000561

Bice, K. L., & Marotzke, J. (2002). Could changing ocean circulation have destabilized methane hydrate at the Paleocene/Eocene boundary? *Paleoceanography and Paleoclimatology*, *17*(2), 8.1–8.13.

Bopp, L., Resplandy, L., Orr, J. C., Doney, S. C., Dunne, J. P., Gehlen, M., et al. (2013). Multiple stressors of ocean ecosystems in the 21st century: Projections with CMIP5 models. *Biogeosciences*, *10*(10), 6225–6245. https://doi.org/10.5194/bg-10-6225-2013

Bowen, G. J., Maibauer, B. J., Kraus, M. J., Rohl, U., Westerhold, T., Steimke, A., et al. (2015). Two massive, rapid releases of carbon during the onset of the Palaeocene-Eocene thermal maximum. *Nature Geoscience*, *8*(1), 44–47. https://doi.org/10.1038/ngeo2316

Caballero, R., & Huber, M. (2013). State-dependent climate sensitivity in past warm climates and its implications for future climate projections. *Proceedings of the National Academy of Sciences*, *110*(35), 14,162–14,167. https://doi.org/10.1073/pnas.1303365110

Chen, Z., Ding, Z., Yang, S., Zhang, C., & Wang, X. (2016). Increased precipitation and weathering across the Paleocene-Eocene Thermal Maximum in central China. *Geochemistry, Geophysics, Geosystems*, *17*, 2286–2297. https://doi.org/10.1002/2016GC006333

Colosimo, A. B., Bralower, T. J., & Zachos, J. C. (2006). Evidence for lysocline shoaling at the Paleocene/Eocene thermal maximum on shatsky rise, northwest pacific. In T. J. Bralower, I. Premoli Silva, & M. J. Malone (Eds.), *Proceedings of the Ocean Drilling Program, Scientific Results*, 198. College Station, TX: Texas A & M University.

Dickens, G. R., O'Neil, J. R., Rea, D. K., & Owen, R. M. (1995). Dissociation of oceanic methane hydrate as a cause of the carbon isotope excursion at the end of the Paleocene. *Paleoceanography*, *10*(6), 965–971. https://doi.org/10.1029/95PA02087

Dunkley Jones, T., Lunt, D. J., Schmidt, D. N., Ridgwell, A., Sluijs, A., Valdes, P. J., & Maslin, M. (2013). Climate model and proxy data constraints on ocean warming across the Paleocene-Eocene Thermal Maximum. *Earth-Science Reviews*, *125*(0), 123–145.

Gibbs, S. J., Bown, P. R., Sessa, J. A., Bralower, T. J., & Wilson, P. A. (2006). Nannoplankton extinction and origination across the Paleocene-Eocene Thermal Maximum. *Science*, *314*(5806), 1770–1773. https://doi.org/10.1126/science.1133902

Gibbs, S. J., Bralower, T. J., Bown, P. R., Zachos, J. C., & Bybell, L. M. (2006). Shelf and open-ocean calcareous phytoplankton assemblages across the Paleocene-Eocene Thermal Maximum: Implications for global productivity gradients. *Geology*, *34*(4), 233–236.

Giorgetta, M. A., Jungclaus, J., Reick, C. H., Legutke, S., Bader, J., Böttinger, M., et al. (2013). Climate and carbon cycle changes from 1850 to 2100 in MPI-ESM simulations for the Coupled Model Intercomparison Project phase 5. *Journal of Advances in Modeling Earth Systems*, *5*, 572–597. https://doi.org/10.1002/jame.20038

González, M. F., Ilyina, T., Sonntag, S., & Schmidt, H. (2018). Enhanced rates of regional warming and ocean acidification after termination of large-scale ocean alkalinization. *Geophysical Research Letters*, *45*, 7120–7129. https://doi.org/10.1029/2018GL077847

Hague, A. M., Thomas, D. J., Huber, M., Korty, R., Woodard, S. C., & Jones, L. B. (2012). Convection of North Pacific deep water during the early Cenozoic. *Geology*, *40*(6), 527–530.

Heinze, M., & Ilyina, T. (2015). Ocean biogeochemistry in the warm climate of the late Paleocene. *Climate of the Past*, *11*(1), 63–79. https://doi.org/10.5194/cp-11-63-2015

Heinze, C., Maier-Reimer, E., Winguth, A. M. E., & Archer, D. (1999). A global oceanic sediment model for long-term climate studies. *Global Biogeochemical Cycles*, *13*(1), 221–250. https://doi.org/10.1029/98GB02812

Hoenisch, B., Ridgwell, A., Schmidt, D. N., Thomas, E., Gibbs, S. J., Sluijs, A., et al. (2012). The geological record of ocean acidification. *Science*, *335*(6072), 1058–1063.

Huber, M, & Caballero, R. (2011). The early Eocene equable climate problem revisited. *Climate of the Past Discussions*, *7*, 241–304.

Huber, M., Sloan, L. C., & Shellito, C. J. (2003). Early Paleogene oceans and climate: A fully coupled modeling approach using the NCAR CCSM. In B. Schmitz, E. Thomas, S. Gingerich, & S. L. Wing (Eds.), *Causes and consequences of globally warm climates in the Paleogene, Geological Society of America, Special Paper* (Vol. 369). Boulder, CO: Geological Society of America.

IPCC (2013). *Climate change 2013: The physical science basis. Contribution of working group I to the fifth assessment report of the intergovernmental panel on climate change*. Cambridge, United Kingdom and New York, NY: Cambridge University Press. https://doi.org/10.1017/CBO9781107415324

Ilyina, T., Six, K. D., Segschneider, J., Maier-Reimer, E., Li, H., & Nunez-Riboni, I. (2013). Global ocean biogeochemistry model HAMOCC: Model architecture and performance as component of the MPI-Earth system model in different CMIP5 experimental realizations. *Journal of Advances in Modeling Earth Systems*, *5*, 287–315. https://doi.org/10.1029/2012MS000178

Ilyina, T., & Zeebe, R. E. (2012). Detection and projection of carbonate dissolution in the water column and deep-sea sediments due to ocean acidification. *Geophysical Research Letters*, *39*, L06606. https://doi.org/10.1029/2012GL051272

Ilyina, T., Zeebe, R. E., Maier-Reimer, E., & Heinze, C. (2009). Early detection of ocean acidification effects on marine calcification. *Global Biogeochemical Cycles*, *23*, GB1008. https://doi.org/10.1029/2008GB003278

Kelly, D. C., Nielsen, T. M., McCarren, H. K., Zachos, J. C., & Röhl, U. (2010). Spatiotemporal patterns of carbonate sedimentation in the South Atlantic: Implications for carbon cycling during the Paleocene-Eocene thermal maximum. *Palaeogeography, Palaeoclimatology, Palaeoecology*, *293*(1), 30–40.

Kennett, J. P., & Stott, L. D. (1991). Abrupt deep-sea warming, palaeoceanographic changes and benthic extinctions at the end of the Palaeocene. *Nature*, *353*(6341), 225–229. https://doi.org/10.1038/353225a0

Le Quéré, C., Andrew, R. M., Friedlingstein, P., Sitch, S., Hauck, J., Pongratz, J., et al. (2018). Global carbon budget 2018. *Earth System Science Data*, *10*(4), 2141–2194. https://doi.org/10.5194/essd-10-2141-2018

Lunt, D. J., Dunkley Jones, T., Heinemann, M., Huber, M., LeGrande, A., Winguth, A., et al. (2012). A model-data comparison for a multi-model ensemble of early Eocene atmosphere-ocean simulations: EoMIP. *Climate of the Past*, *8*(5), 1717–1736. https://doi.org/10.5194/cp-8-1717-2012

Lunt, D. J., Valdes, P. J., Jones, T. D., Ridgwell, A., Haywood, A. M., Schmidt, D. N., et al. (2010). CO2-driven ocean circulation changes as an amplifier of Paleocene-Eocene Thermal Maximum hydrate destabilization. *Geology*, *38*(10), 875–878.

Mauritsen, T., Stevens, B., Roeckner, E., Crueger, T., Esch, M., Giorgetta, M., et al. (2012). Tuning the climate of a global model. *Journal of Advances in Modeling Earth Systems*, *4*, M00A01. https://doi.org/10.1029/2012MS000154

McInerney, F. A., & Wing, S. L. (2011). The Paleocene-Eocene Thermal Maximum: A perturbation of carbon cycle, climate, and biosphere with implications for the future. *Annual Review of Earth and Planetary Sciences*, *39*(1), 489–516. https://doi.org/10.1146/annurev-earth-040610-133431

Meraner, K., Mauritsen, T., & Voigt, A. (2013). Robust increase in equilibrium climate sensitivity under global warming. *Geophysical Research Letters*, *40*, 5944–5948. https://doi.org/10.1002/2013GL058118

Nunes, F., & Norris, R. D. (2006). Abrupt reversal in ocean overturning during the Palaeocene/Eocene warm period. *Nature*, *439*(7072), 60–63.

Palike, C., Delaney, M. L., & Zachos, J. C. (2014). Deep-sea redox across the Paleocene-Eocene thermal maximum. *Geochemistry, Geophysics, Geosystems*, *15*, 1038–1053. https://doi.org/10.1002/2013GC005074

Panchuk, K., Ridgwell, A., & Kump, L. R. (2008). Sedimentary response to Paleocene-Eocene Thermal Maximum carbon release: A model-data comparison. *Geology*, *36*(4), 315–318. https://doi.org/10.1130/G24474A.1

Penman, D. E., Hoenisch, B., Zeebe, R. E., Thomas, E., & Zachos, J. C. (2014). Rapid and sustained surface ocean acidification during the Paleocene-Eocene Thermal Maximum. *Paleoceanography*, *29*, 357–369. https://doi.org/10.1002/2014PA002621

Popp, M., Schmidt, H., & Marotzke, J. (2016). Transition to a moist greenhouse with CO_2 and solar forcing. *Nature Communications*, *7*, 10627. https://doi.org/10.1038/ncomms10627

Ridgwell, A., & Schmidt, D. N. (2010). Past constraints on the vulnerability of marine calcifiers to massive carbon dioxide release. *Nature Geoscience*, *3*(3), 196–200.

Séférian, R., Gehlen, M., Bopp, L., Resplandy, L., Orr, J. C., Marti, O., et al. (2016). Inconsistent strategies to spin up models in CMIP5: Implications for ocean biogeochemical model performance assessment. *Geoscientific Model Development*, *9*(5), 1827–1851. https://doi.org/10.5194/gmd-9-1827-2016

Sluijs, A., Bijl, P. K., Schouten, S., Röhl, U., Reichart, G.-J., & Brinkhuis, H. (2011). Southern ocean warming, sea level and hydrological change during the Paleocene-Eocene Thermal Maximum. *Climate of the Past*, *7*(1), 47–61. https://doi.org/10.5194/cp-7-47-2011

Sluijs, A., Schouten, S., Pagani, M., Woltering, M., Brinkhuis, H., Damsté, J. S. S., et al. (2006). Subtropical Arctic Ocean temperatures during the Palaeocene/Eocene thermal maximum. *Nature*, *441*(7093), 610–613. https://doi.org/10.1038/nature04668

Thomas, E. (2007). Cenozoic mass extinctions in the deep sea: What perturbs the largest habitat on Earth? *Geological Society of America Special Papers*, *424*, 1–23. https://doi.org/10.1130/2007.2424(01)

Thomas, D. J., Bralower, T. J., & Jones, C. E. (2003). Neodymium isotopic reconstruction of late Paleocene–early Eocene thermohaline circulation. *Earth and Planetary Science Letters*, *209*(3–4), 309–322.

Thomas, D. J., Zachos, J. C., Bralower, T. J., Thomas, E., & Bohaty, S. (2002). Warming the fuel for the fire: Evidence for the thermal dissociation of methane hydrate during the Paleocene-Eocene thermal maximum. *Geology*, *30*(12), 1067–1070.

Tripati, A., & Elderfield, H. (2005). Deep-sea temperature and circulation changes at the Paleocene-Eocene Thermal Maximum. *Science*, *308*(5730), 1894–1898. https://doi.org/10.1126/science.1109202

Turner, S. K., Hull, P. M., Kump, L. R., & Ridgwell, A. (2017). A probabilistic assessment of the rapidity of PETM onset. *Nature Communications*, *8*(1), 353.

Winguth, A. M. E., Thomas, E., & Winguth, C. (2012). Global decline in ocean ventilation, oxygenation, and productivity during the Paleocene-Eocene Thermal Maximum: Implications for the benthic extinction. *Geology*, *40*(3), 263–266. https://doi.org/10.1130/G32529.1

Zachos, J. C., Dickens, G. R., & Zeebe, R. E. (2008). An early Cenozoic perspective on greenhouse warming and carbon-cycle dynamics. *Nature*, *451*(7176), 279–283. https://doi.org/10.1038/nature06588

Zachos, J. C., Röhl, U., Schellenberg, S. A., Sluijs, A., Hodell, D. A., Kelly, D. C., et al. (2005). Rapid acidification of the ocean during the Paleocene-Eocene Thermal Maximum. *Science*, *308*(5728), 1611–1615. https://doi.org/10.1126/science.1109004

Zachos, J. C., Wara, M. W., Bohaty, S., Delaney, M. L., Petrizzo, M. R., Brill, A., et al. (2003). A transient rise in tropical sea surface temperature during the Paleocene-Eocene Thermal Maximum. *Science*, *302*(5650), 1551–1554. https://doi.org/10.1126/science.1090110

Zeebe, R. E., & Zachos, J. C. (2007). Reversed deep-sea carbonate ion basin gradient during Paleocene-Eocene Thermal Maximum. *Paleoceanography*, *22*, PA3201. https://doi.org/10.1029/2006PA001395

Zeebe, R. E., Zachos, J. C., & Dickens, G. R. (2009). Carbon dioxide forcing alone insufficient to explain Palaeocene-Eocene Thermal Maximum warming. *Nature Geoscience*, *2*(8), 576–580. https://doi.org/10.1038/ngeo578